AUT Journal of Electrical Engineering

AUT J. Elec. Eng., 58(3) (2026) 489-508
DOI: 10.22060/eej.2026.25230.5872

NGOA Assisted Neural Network MPPT for Grid-Connected PV System with Soft-Clamp X-Gain Boost Converter

Viswaprakash Babu[1]*, T. Sridevi[2], M. J. Murali[3], J. Gnanavel[4], D. Dinesh[5], M. Balasubramanian[6]

[1] Department of Electrical and Electronics Engineering, Kaveri University, Gouraram, Siddipet, Telangana, India, Pin- 502279.
[2] Department of Electrical and Electronics Engineering, Peri Institute of Technology, Chennai, 600048, India.
[3] Department of Electrical and Electronics Engineering, Bharath Institute of Science and Technology, Bharath Institute of Higher Education and Research, Chennai 600 073, India.
[4] Department of Electrical and Electronics Engineering, Achariya College of Engineering Technology, Pondicherry.
[5] Department of Mechatronics Engineering, Chennai Institute of Technology, Chennai 600069.
[6] Department of Electrical and Electronics Engineering, Government College of Engineering, Tirunelveli 627007, Tamilnadu, India.

ABSTRACT: This work presents an intelligent Photovoltaic (PV) grid integration system employing a Northern Goshawk Optimization Algorithm (NGOA)-based Radial Basis Function Neural Network (RBFNN) for Maximum Power Point Tracking (MPPT) and Soft Clamp X-Gain Boost (SC-XGB) converter for enhanced voltage regulation. The proposed system aims to optimize energy harvesting from a PV source and ensure stable power delivery to a three-phase grid. The RBFNN is trained offline using comprehensive PV datasets and directly predicts the optimal duty cycle from measurable PV inputs during real-time operation, eliminating the need for auxiliary MPP pre-estimation algorithms, while NGOA enhances the RBFNN's learning capability by fine-tuning its weights and biases for rapid and accurate MPPT performance even under varying irradiance and temperature conditions. PV output is connected to SC-XGB, which efficiently raises the Direct Current (DC) voltage and is thus controlled by Pulse Width Modulation (PWM) signals which are generated according to MPPT output. Regulated DC output is then transformed into a three-phase Alternating Current (AC) by a Voltage Source Inverter (VSI), the output of which is taken through an LC filter to reduce harmonics before the power is fed into the grid. Simulation is done in MATLAB showing the capacity of NGOA-RBFNN to track Maximum Power Point (MPP) at very high speed and accuracy. The system achieves superior voltage regulation of 95.24% efficiency, reduced Total Harmonic Distortion (THD) and enhanced dynamic performance over traditional MPPT control methods.

Review History:
Received: Dec. 05, 2025
Revised: Feb. 20, 2025
Accepted: May, 04, 2025
Available Online: Jul. 01, 2026

Keywords:
PV System
Soft Clamp X-gain Boost Converter
NGOA-based RBFNN MPPT
Three-Phase VSI
Grid System

1- Introduction

Grids have become one of the best viable methods to solve energy issues including the lack of energy supplies and the problem of energy consumption and production being out of balance. As a result of these systems being locally controlled, they give a lot of advantages to communities, such as lowering the emission of greenhouse gases, increasing energy safety and making power infrastructure more reliable and less vulnerable [1]. In fact, recent advances in microgrid technology have been mainly aimed at increasing the operational efficiency and overall performance of system. One notable progress area is the integration of RESs like solar, wind and biomass, as a way of broadening the energy base. Furthermore, by storing extra energy for utilization during times of low renewable generation, advanced battery systems and other cutting-edge energy storage technologies, are essential for grid stabilization [2].

Among different sustainable energy choices, solar power is undoubtedly one of the most popular. It has been gaining recognition as a clean and a green energy source, among other reasons that include its high energy conversion efficiency and low maintenance need [3]. PV installations are solar-energy based electric power generation systems that work by extracting sunlight and through PV effect converting it into electrical energy in solar cells [4]. Each solar cell usually consist of a semiconductor-based PN junction that is specifically engineered for the energy conversion process. The performance of PV installations is influenced by a number of factors, including the geographical location, shading, and prevailing climate in the area. Furthermore, the technical composition of PV components and the inclination angle of the PV panel also influence the output power of the system [5]. Given that the output voltage of PV cells is generally too low to be used for a leap of power operation of photovoltaic-

*Corresponding author's email: viswaprakash125@yahoo.com

Copyrights for this article are retained by the author(s) with publishing rights granted to Amirkabir University Press. The content of this article is subject to the terms and conditions of the Creative Commons Attribution 4.0 International (CC-BY-NC 4.0) License. For more information, please visit https://www.creativecommons.org/licenses/by-nc/4.0/legalcode.

based EVs, first of all, basic hard-switching converters are usually inefficient in producing the required energy [6].

To overcome this drawback, soft-switching converters are the right choice because of their high efficiency and low power loss. For instance, a step-up DC-DC converter raises the voltage to a higher level. Still, getting a high voltage from a standard boost converter in very demanding applications is not easy; the performance needs to be kept at the best level [7]. Besides, solar-powered grid systems are in need of converters with very high power ratings in order to provide the specified voltage and current levels. The Interleaved Boost Converter (IBC) conFiguration is in use, in view of the fact that more and more emphasis is being placed on the standards of energy efficiency, IBC is one of the few good choices that handle the tough design problems. However, the more phases there are, the higher the total cost of the topology. Therefore, the phase count and system robustness are the main trade-offs as a result of the very large increase in components required [8]. Integrating a quadratic boost converter with a PV system is one way to achieve a high voltage conversion ratio and maintain high efficiency over a wide input voltage range. However, the need for multiple passive and active components increases the design complexity [9]. The switched-inductor boost converter is a three-diode and two-inductor arrangement. In this, the output voltage is significantly stepped up by the inductors being charged in parallel and discharged in series. Both inductors have a common magnetic core, and the voltage stress on the switch and diodes equals the output voltage [10]. However, this converter has higher conduction losses. Hence, in addition to converter development, smart MPPT methods need to be implemented to get the best power extraction from fast-changing environmental conditions.

To make the PV systems more adaptable to the changes in the irradiance conditions, advanced architectures have been proposed that use step-size adjustment methods, dual-parameter perturbation schemes and contain features that limit the deviations in output power [11]. However, the PV systems' output is often degraded by the surrounding conditions such as changing irradiance, temperature variations, and Partial Shading Conditions (PSCs) [12]. By developing different MPPT techniques, PV systems are harnessing their capability to frequently perform at their maximum power level. Various MPPT technologies, such as intelligent, metaheuristic, traditional, and their hybrid combinations, are widely scrutinized and have been the focus of research [13]. Perturb and Observe (P&O) and Incremental Conductance (INC) are two of the most popular traditional MPPT techniques due to their easy designs and implementations. However, these methods tend to lose their efficiency under fast, changing environmental conditions and Partial Shading that are typical of PV installations [14]. As a result, AI-based RBFNN methods have been developed and introduced to overcome these limitations, which provide higher speed and accuracy of tracking under real- time operating conditions.

1- 1- Related works

The efficiency of the tracking abilities is further improved by the optimization algorithms, fine-tuning the controller parameters in tracking MPP. **Abdelilah Hilali *et al* (2022)** have presented that the Genetic Algorithm (GA) operates on natural selection and evolutionary genetics, making it effective for global optimization tasks. However, its computational complexity often limits its suitability for real-time applications [15]. **Adel O. Baatiah *et al* (2023)** have implemented Particle Swarm Optimization (PSO), which utilizes swarm intelligence to navigate solution spaces; however gets trapped in local optima, especially in high-dimensional scenarios [16]. In contrast, **Othman m. Hussein Anssari *et al* (2024)** have implemented Adaptive Particle Optimization (APO), which offers a distinct advantage through its responsiveness to real-time variations, such as changes in solar irradiance or fluctuating load demands [17]. **Mehrdad Ahmadi Kamarposht *et al* (2022)** have developed a Whale Optimization Algorithm (WOA) based on meta-heuristics, designed to tackle nonlinear problems involving multiple objectives [18]. Unlike GA, which often requires re-initialization in dynamic settings, and PSO, which adapts more slowly, APO employs a dynamic optimization strategy that enables rapid and efficient energy allocation adjustments; however, it still suffers from premature convergence and increased computational overhead due to its adaptive mechanisms. Similarly, the exploitation phase of WOA gets sluggish, and it risks getting trapped in local optima, especially in high-dimensional or noisy environments.

1- 2- Research Gap

Many topologies of a converter have been introduced to increase the voltage gain of a PV; however, several of these schemes have problems, including increased conduction losses, high voltage stress, or a large number of components that increase the cost and complexity, etc. Conventional MPPT methods are easy to understand and implement, but are not able to give improved performance under rapidly changing irradiance and partial shading conditions. AI-based and metaheuristic controllers in use nowadays have made the system more adaptable, but the problems of computational overhead, premature convergence and slow dynamic response are still present. Hence, these issues point out the necessity of advanced converter architectures combined with smart MPPT techniques that are capable of delivering efficient, stable and high-gain operation even in a wide variety of environmental conditions.

1- 3- Contributions

The proposed PV-powered grid system contributions are listed below:

- PV system serves as the main source of renewable energy, converting solar irradiance into electrical power to be fed into the grid.
- A SC-XGB converter boosts the low and fluctuating DC voltage of the PV system to a high and steady level for efficient power delivery.
- Northern goshawk optimized RBFNN MPPT tracks MPP quickly in dynamic conditions, achieving maximum

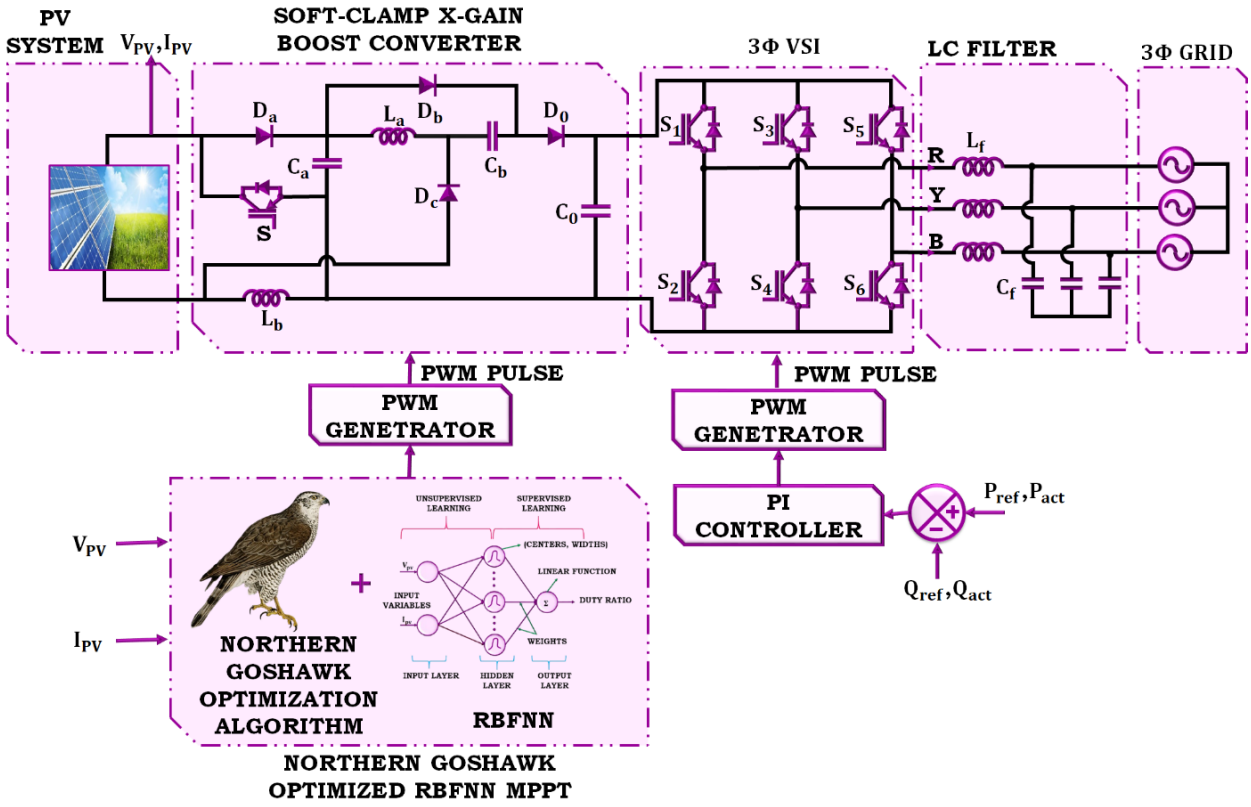

Fig. 1. Proposed PV-powered grid system.

energy harvesting.

- VSI regulates the increased DC voltage into synchronized three-phase AC power for grid feed.
- LC filter suppresses the inverter output by suppressing high-frequency harmonics, providing clean and grid-quality AC power supply.

1- 4- Organization

This paper's remaining sections are organized as follows: The proposed system and its essential elements are introduced in Section II. Section III presents detailed modelling of the system, including PV system dynamics, the SC-XGB converter, the NGOA-RBFNN for MPPT, and grid synchronization mechanisms. Section IV discusses results and provides a comprehensive analysis of system performance. Finally, Section V concludes the study with key findings and insights.

2- Proposed System Description

A block diagram of the proposed PV-powered grid-connected system is demonstrated in Fig. 1, which demonstrates a high-performance control and conversion architecture integrating a northern goshawk-tuned RBFNN for MPPT and SC-XGB converter to improve voltage conversion efficiency.

PV array is the primary source of renewable power, providing a variable DC voltage and current (V_{PV}) and (I_{PV}) based on solar irradiance and temperature conditions. SC-XGB converter, a high-efficiency converter that can provide a large voltage gain and also sustain high efficiency for a wide range of input voltages. The relatively low and varying DC voltage from the PV array is boosted to a high DC voltage (V_{DC}), which is ideal for interfacing with the grid. The electrical parameters are monitored continuously and entered into the northern goshawk-optimized RBFNN MPPT controller. The northern goshawk optimization algorithm improves the learning and adaptability of the RBFNN so that it tracks MPP correctly and quickly under dynamic environmental conditions. PWM signals control the switching mode of the converter so that the voltage conversion process is controlled with great accuracy. After boosting DC voltage, it is supplied to a three-phase VSI, which converts DC power into three-phase AC power suitable for grid standards. The inverter is a vital part of the system, as it synchronizes the output with the voltage and frequency of grid. To keep power quality and reduce harmonic distortions, the AC output of the inverter is given through an LC filter. This filter gets rid of the high-frequency components, and the resulting waveform is smooth. A clean sinusoidal output conforming to the

grid requirements is thus obtained. The filtered AC power is supplied to the three-phase electrical grid (3φ GRID) and adds to the overall supply of energy. For grid stability and to provide efficient power transfer, the system uses a closed-loop control scheme with a PI controller. PI controller calculates the difference between the reference and actual values and produces corrective signals to modify the inverter operation appropriately. These control signals are applied to a second PWM generator, which controls inverter switches by modulating them for desired power flow and reactive power compensation.

3- Proposed System Modelling

3- 1- PV System Modelling

Electricity is produced by converting sunlight into electrical energy through the photovoltaic effect. The single-diode equivalent circuit of a photovoltaic PV cell is shown in Fig. 2.

The relationship between output current and voltage of a solar cell is governed by the following equation:

$$I_{PV} = I_{ph} - I_0\left[exp\left(\frac{q\cdot\left(V_{PV}+I\cdot R_S\right)}{n\cdot K\cdot T}\right)-1\right] - \frac{V_{PV}+R_S\cdot I}{R_{sh}} \quad (1)$$

where T is cell temperature in Kelvin, R_S is series resistance, R_{sh} is shunt resistance, q is electron charge (1.6×10^{-19} C), K is Boltzmann constant (1.38×10^{-23} J/K), I_{PV} is PV cell's output current, I_{ph} is photo-generated current (proportional to solar irradiance G), I_0 is the diode saturation current, and q is the electron charge.

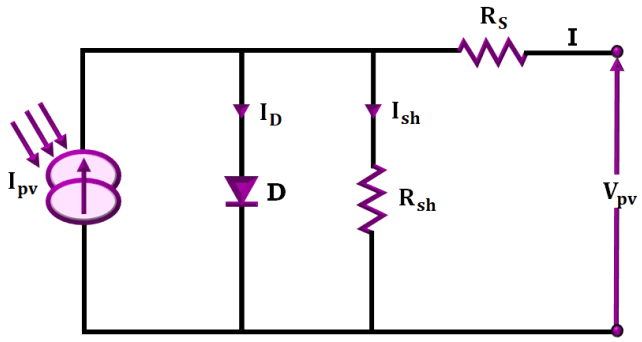

Fig.2. Equivalent PV circuit.

PV module's I–V and P–V characteristics are revealed in Fig. 3. (a) and Fig. 3. (b) at various ambient temperatures and solar irradiance levels. The photo-current grows proportionately with increasing irradiance, which raises the PV module's output power.

The photo-current I_{PV} also be expressed as:

$$I_{PV} = I_{CC}^{*}\left(\frac{G}{G^{*}}\right)+\alpha_1\left(T-T^{*}\right) \quad (2)$$

Where, α_1 is the temperature coefficient (A/°C), G^{*} is reference irradiance (1 kW/m²), T^{*} is reference temperature (25°C), and I_{CC}^{*} is the short-circuit current at reference circumstances (25°C, 1 kW/m²). An important factor in PV performance is temperature. The following provides the open-circuit voltage V_{oc} :

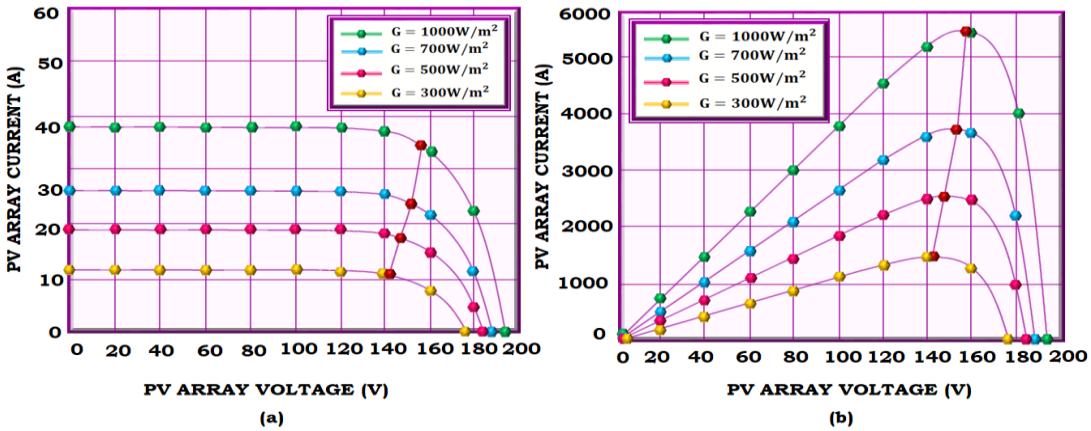

Fig.3. (a) I-V (b) P-V characteristic of PV array.

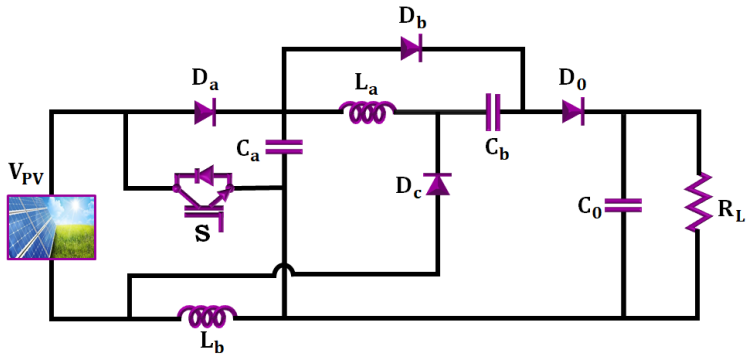

Fig.4. Proposed SC-XGB Converter.

$$V_{oc} = V_{oc}^{*} + \alpha_2 \left(T - T^{*}\right) - \left(I_{CC} - I_{CC}^{*}\right) \cdot R_S \tag{3}$$

Where, V_{oc} is the open-circuit voltage at reference conditions, α_2 is the temperature coefficient (V/°C). Due to the nonlinear nature of PV output characteristics and their dependency on irradiance and temperature, it's essential to operate the module at its MPP. To achieve this, an MPPT controller is employed, typically managing a switched-mode DC-DC converter to ensure optimal load matching.

3- 2- Soft Clamp X-Gain Boost Converter

Due to PV low and unreliable power generation, a SC-XGB-based DC-DC converter is equipped for boosting voltage levels. Schematic of the proposed SC-XGB is illustrated in Fig. 4. The converter structure comprises two inductors (L_a, L_b), diodes (D_a, D_b, D_c, D_0), input capacitors (C_a, C_b), output capacitor (C_0), and a single power switch (S). The switch is driven by a single PWM control signal, simplifying the overall control strategy and minimizing the requirement for multiple gate driver circuits.

Essentially, the proposed topology is a very good medium through which the voltage conversion ratio is effectively enhanced. At the same time, excellent high-gain operation is achieved with good efficiency. Thus, the converter that has been proposed is used very well in renewable energy applications such as PV systems, where it is necessary to have both high efficiency and a large voltage step-up capability. The Continuous Conduction Mode (CCM) operation of the converter is described in the subsequent section.

The converter is in two different modes based on the switching signal of the power switch (S). These are switch ON mode and switch OFF mode. For CCM, currents through inductors are non-zero, supporting smooth energy transfer for the entire switching cycle. Energy flows alternately from the PV source to the inductors and then to the load through capacitors and diodes and facilitates achieving high step-up voltage gain.

Mode 1 (Switch ON, $0 \le t \le DT$): When switch (S) is ON, Fig. 5(a), (D_a) and (D_0) are reverse-biased, and (D_b) and (D_C) are forward-biased. (V_{PV}) charges (L_a) and (L_b), and also stores energy in capacitor (C_a). At the same time, the output capacitor (C_0) delivers power to load. This action boosts energy stored in both inductors throughout ON duration.

Voltage equations for Mode-1 are obtained applying Kirchhoff's Voltage Law (KVL):

$$V_{La} = V_{PV} + V_{Ca} = V_{Cb} \tag{4}$$

$$V_{Lb} = V_{PV} \tag{5}$$

The inductor (L_b) is directly charged from the source during ON interval so its instantaneous voltage equal s (V_{PV}).

Mode 2 (Switch OFF, $T \le t \le T$): When (S) is OFF, Fig. 5(b), (D_a) and (D_0) are forward-biased and (D_b) and (D_C) is reverse-biased. In this condition, stored energy from (L_a) and (L_b) and (C_a) is dissipated and delivered to the output via (C_b) and (D_0). Therefore, both inductors deliver their energy to the load, considerably increasing the output voltage.

When the switch is OFF, the diodes reconFigure, and the stored energies discharge to the output. Apply KVL around the loop containing

$$V_{Ca} - V_{La} + V_{Cb} - V_0 \tag{6}$$

Rearranging the equations,

$$-V_{La} = V_0 - V_{Ca} - V_{Cb} = 0 \tag{7}$$

Use the relation from Mode-1 eqn (4) into eqn (7)

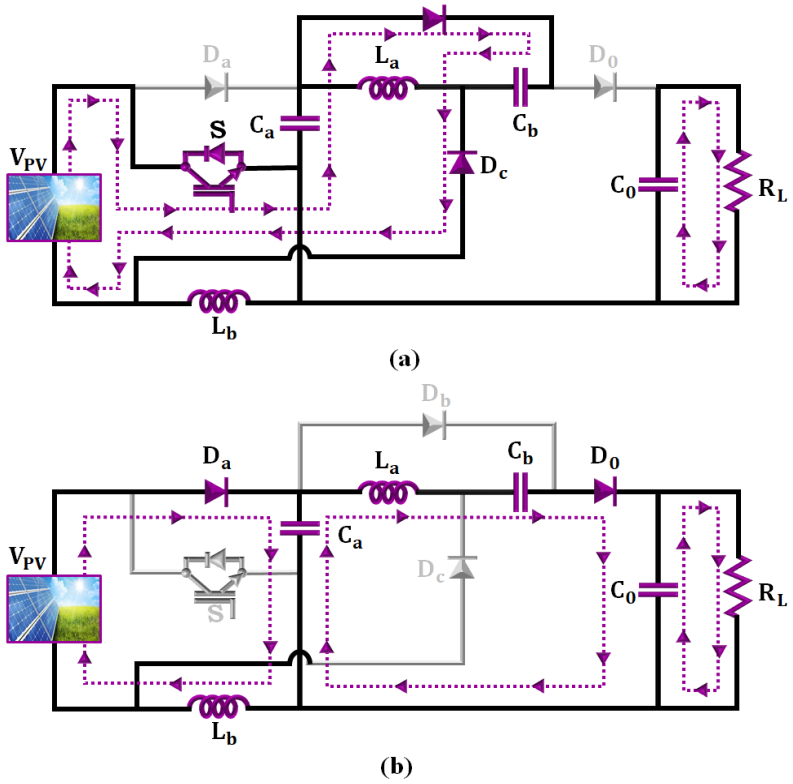

Fig.5. (a) Mode 1 (b) Mode 2 operation of soft clamp x-gain boost.

$$-V_{La} = V_0 - V_{Ca} - (V_{PV} + V_{Ca}) \tag{8}$$

$$V_{La} = V_{PV} + 2V_{Ca} - V_0 \tag{9}$$

$$V_{Lb} = V_{PV} - V_{Ca} \tag{10}$$

Next, the voltage across L_b in mode-2 is a difference between the input and the C_a voltage because of the conduction path:

$$V_{PV} \cdot D = (V_{PV} - V_{Ca})(1-D) = 0 \tag{11}$$

Apply the volt-second balance on L_b (average over one switching period must be zero):

During ON (duration D) $\left(V_{Lb(on)} = V_{PV}\right)$

During OFF (duration 1-D): $\left(V_{Lb(off)} = V_{PV} - V_{Ca}\right)$

$$V_{Ca} = \frac{V_{PV}}{1-D} \tag{12}$$

$$(V_{PV} + V_{Ca})D + (2V_{Ca} + V_{PV} - V_0)(1-D) = 0 \tag{13}$$

$$-V_0(1-D) + V_{Ca}(2-D) + V_{PV} = 0 \tag{14}$$

Substituting $V_{Ca} = \frac{V_{PV}}{1-D}$

$$V_0(1-D) = \frac{V_{PV}(3-2D)}{1-D} + V_{PV} \tag{15}$$

Final voltage gain of proposed SC-XGB,

$$\frac{V_0}{V_{PV}} = \frac{(3-2D)}{(1-D)^2} \tag{16}$$

The timing diagram of SC-XGB converter is given in Fig. 6, showcasing the switching sequence and current through the inductors and diodes during each phase, which is crucial to attain the intended high voltage gain and synchronized operation among the converter components.

3- 3- NGOA-based RBFNN MPPT

The proposed RBFNN method effectively estimates a near-optimal duty cycle that positions the PV array close to its MPP. RBFNNs are increasingly used to tackle complex optimization problems, are highly adaptable, and do not require detailed system modelling, relying instead on input–

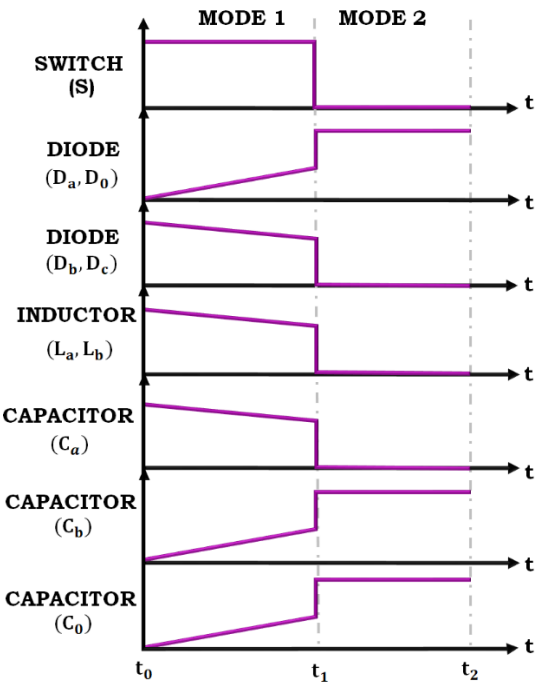

Fig.6. Timing Diagram.

output relationships. RBFNN offers a more efficient structure by modelling nonlinear functions based on the scalar product of inputs and weights, enabling it to search for the best-fitting surface in a multidimensional space.

RBFNN comprises three layers, Fig. 7 input layer, hidden layer with Gaussian activation functions, output layer with linear activation functions.

Unsupervised Learning (Input to Hidden Layer)

Centre (μ) and Width (σ) parameters for each hidden neuron are determined using the K-means clustering algorithm. Each training input is assigned to the nearest cluster by z

$$Euclidean\ distance, E_D(x,c) = \sqrt{\sum_{i=1}^{n}(x_i - c_i)^2} \tag{17}$$

Cluster centres are updated iteratively until they stabilize. The width parameter (σ_m) for each hidden neuron is calculated as,

$$\sigma_m = \frac{1}{P}\sqrt{\sum_{m=1}^{P}|\mu_{m+1} - \mu_m|^2} \tag{18}$$

These parameters are then used in the Gaussian activation function to compute the hidden layer outputs:

$$\sigma_j = \frac{1}{\sigma\sqrt{2\pi}} exp\left[\frac{-(x-\mu)^2}{2\sigma^2}\right] \tag{19}$$

The weight matrix between the hidden and output layers is trained. Net output is computed as:

$$net_k = \sum_{k=1}^{n}\sum_{j=1}(w_{jk} + o_j) \tag{20}$$

Since the output layer uses a linear activation function,

$$o_k = net_k \tag{21}$$

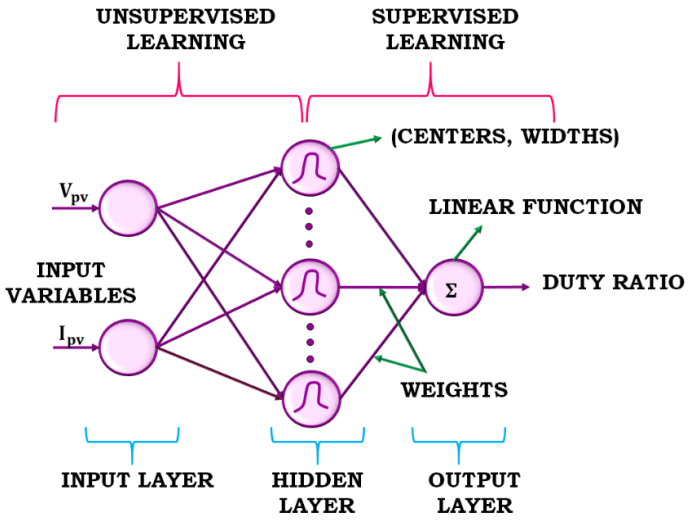

Fig.7. RBFNN Architecture.

Error (ε) between the target and actual output is:

$$error, \varepsilon = t_k - o_k \tag{22}$$

This training continues until the error falls within acceptable limits. Here, the RBFNN model does not rely on an externally pre-estimated MPP during its real-time operation. A PV dataset of a comprehensive nature is used to train the network offline. These datasets are synthetically generated by varying the irradiance and temperature conditions. When RBFNN is put online, it takes only those measurable PV parameters, which are obtained from the module, such as array voltage and current as inputs. So, with knowledge of PV voltage and current, RBFNN identifies a suitable duty cycle that brings PV array power to the maximum point.

The performance of the RBFNN in tracking maximum power is further enhanced by the integration of NGOA, which draws inspiration from the northern goshawk's hunting strategy, which involves two primary actions: an immediate strike upon spotting prey, followed by a rapid and agile pursuit. The dual-phase strategy described above is the basis for the mathematical model of the NGOA. The algorithm tries to copy the animal's behaviours of first locating the prey and attacking it followed by a series of actions where the two animals chase and evade.

In the first stage of the algorithm, the goshawk chooses a target by chance within the area it searches, and then it performs a lightning-fast strike. This random selection helps in improving the exploration capability of the algorithm so that it comprehensively covers the search space in search of the best solutions.

The position of the i^{th} goshawk during hunting is denoted by:

$$P_n = X_i, n = 1,2,3,\ldots K, i = 1,2,..n-1,\ n+, K \tag{23}$$

Updated position based on the first phase is:

$$x_{n,k}^{new,p1} = \begin{cases} x_{n,k} + r\left(p_{n,k} - Ix_{n,k}\right), F_{pn} < F_n \\ x_{n,k} + r\left(x_{n,k} - p_{n,k}\right), F_{pn} \geq F_n \end{cases} \tag{24}$$

The new position is accepted if it improves the objective function:

$$x_n = \begin{matrix} x_n^{new,p1}, F_n^{new,p1} < F_n \\ x_n, F_n^{new,p1} \geq F_n \end{matrix} \tag{25}$$

Where, r is a random number in [0,1], I is either 1 or 2, and F_{pn} is the objective function value at the prey position.

Velocity update for the i^{th} goshawk is defined as:

$$V_i = \delta V_i + \mu\left(x_{n,k}^{new,p1} - x_n\right) \tag{26}$$

Where, δ and μ are updated coefficients. In the second phase, the position is further refined using:

$$x_{n,k}^{new,p2} = x_{n,k} + R\left(2r-1\right)x_{n,k} \tag{27}$$

$$R = 0.02\left(1 - \frac{t}{T}\right) \tag{28}$$

Where, t is the current iteration and T is the maximum number of iterations. Updated position is accepted based on:

$$x_n = \begin{cases} x_n^{new,p2}, F_n^{new,p2} < F_n \\ x_n, F_n^{new,p2} \geq F_n \end{cases} \tag{29}$$

The Fig. 8 represents the NGOA-RBFNN optimized MPPT algorithm, highlighting the integration of the northern goshawk optimization algorithm and RBFNN to optimize tracking accuracy and response rate under changing solar irradiance and temperature levels. The final optimized duty cycle is then sent to the PWM generator that produces gating signals for SC-XGB, ensuring increased power delivery from PV system to the connected load.

3- 4- Grid Synchronization

Three-phase VSIs are usually controlled using either voltage control or current control techniques. In grid-connected applications, control is mainly based on current regulation, as shown in Fig. 9. Therefore, the inverter system's performance depends greatly on the accuracy and strength of the current controller used.

Out of many control strategies, the PI controller is the one most commonly used for eliminating current variations. It takes two main inputs: the reference current, which is set by the grid requirements, including active and reactive power, and the actual current coming from the VSI. After calculating the difference between these two signals, the PI controller generates a control signal that changes the operation of the inverter.

This technique keeps harmonic distortion low, current ripple at a minimum, and steady-state behaviour very good, as well as provides a stable switching frequency. Moreover, the PI controller is not model-dependent, so it is not susceptible to changes in system parameters.

Mathematically, a grid-connected inverter's output voltage in the dq-synchronous reference frame is described as:

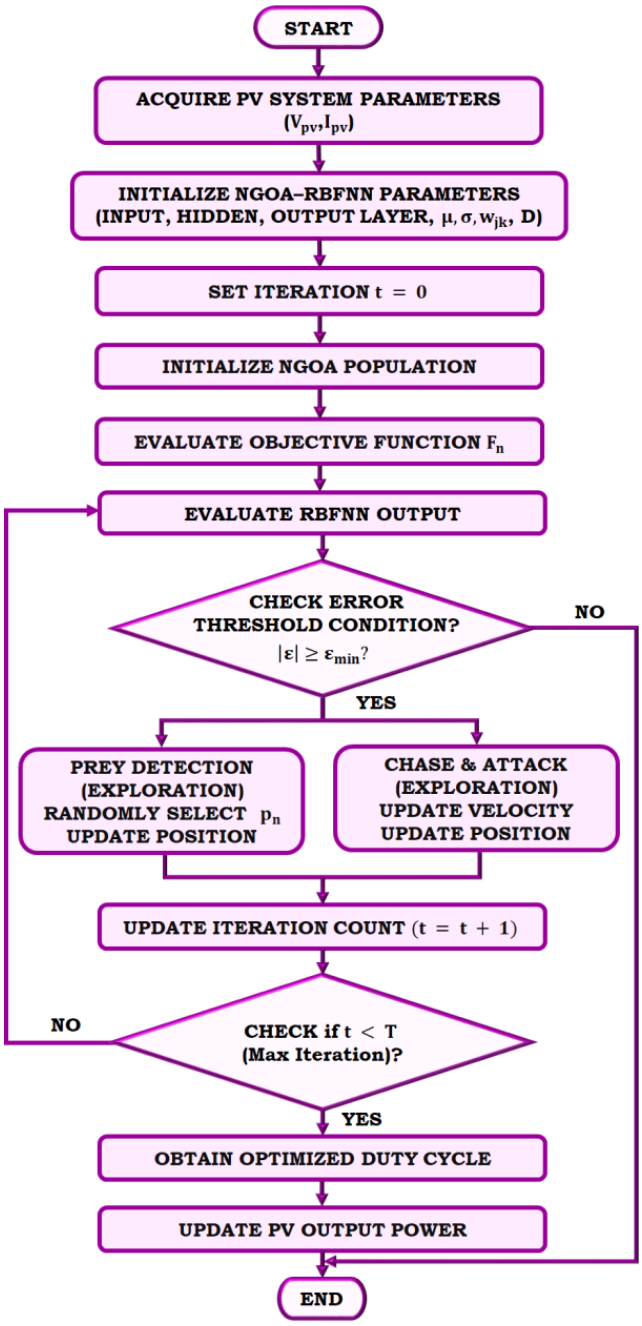

Fig. 8. Flowchart of NGOA-RBFNN MPPT.

$$\begin{bmatrix} u_d \\ u_q \end{bmatrix} = L\frac{d}{dt}\begin{bmatrix} i_d \\ i_q \end{bmatrix} + R\begin{bmatrix} i_d \\ i_q \end{bmatrix} + \omega L\begin{bmatrix} -i_d \\ i_q \end{bmatrix} + \begin{bmatrix} e_d \\ e_q \end{bmatrix} \quad (30)$$

Where, (e_d) and (e_q) are the grid voltage components after Park transformation, (u_d) and (u_q) are the inverter output voltages after transformation, ω is angular frequency and L and R are inductance and resistance between the inverter and the grid.

4- Result and Discussion

This section examines the efficiency of the proposed system, an integration of the SC-XGB converter and NGOA-RBFNN MPPT controller, through MATLAB/Simulink experimentation. Results demonstrate that the system achieves superior efficiency, enhanced voltage gain, and improved MPPT accuracy under varying environmental conditions. Specifications of the PV system and X-gain boost converter used in the simulation are detailed in Table 1.

Case 1: Constant temperature and intensity

Fig. 10 presents the temperature, intensity, voltage, and current waveform of the PV system under constant temperature and irradiance. PV panel temperature remained at 28°C, keeping the semiconductor properties of the solar cells unaltered, so that the voltage output remains constant. The solar irradiance is kept constant at 800 W/m² to deliver a stable and continuous energy supply to the PV array. The solar array exhibits a flat voltage waveform of about 420V throughout the system. The waveform of the input current, which remains constant at around 75A, this steady current flow ensures that the converter is able to deliver power to the grid with minimum loss.

Fig.11 represents the voltage and current response of a northern goshawk optimized-RBFNN MPPT-controlled SC-XGB converter exhibiting a very stable and efficient operating condition. This stability carries over to the SC-XGB, whose output voltage waveform starts around 600 V and stabilizes rapidly with minimal oscillation. The current waveform of the converter also begins about 100A and stabilizes quickly around 50A, demonstrating the fast dynamic response and strong control of the converter under the NGOA-RBFNN MPPT algorithm. The northern goshawk optimized-RBFNN improves this performance by efficiently adjusting to the constant input conditions, so the converter runs at optimal efficiency without overshooting. Essentially, the steady temperature and irradiance provide an optimal condition in which the MPPT and SC-XGB converter are allowed to operate in their best capabilities, leading to predictable and smooth waveforms that indicate a well-controlled and high-performance PV system.

Case 2: Varying temperature and intensity

Fig.12 displays the dynamic behaviour of the PV system, where the environmental conditions start to change, temperature and solar intensity. The system starts in stable conditions: the PV panel is kept at an ambient temperature of approximately 25°C and under an irradiance of 800 W/m². Input voltage and current waveforms are stable during this stage, which means the MPPT controller has locked into the optimum operating point successfully. However, at about 0.3s, temperature and irradiance start increasing, temperature reaches 35°C, and irradiance rises to 980 W/m². This change causes a response in the electrical behaviour of the PV system. With increasing temperature, the voltage of the PV panel generally reduces, which causes a minor reduction in input voltage from 420 V to 400 V. At the same time, the increase in irradiance increases the photocurrent, causing a spike in the input current from 50 A to 60 A. The smooth settling and

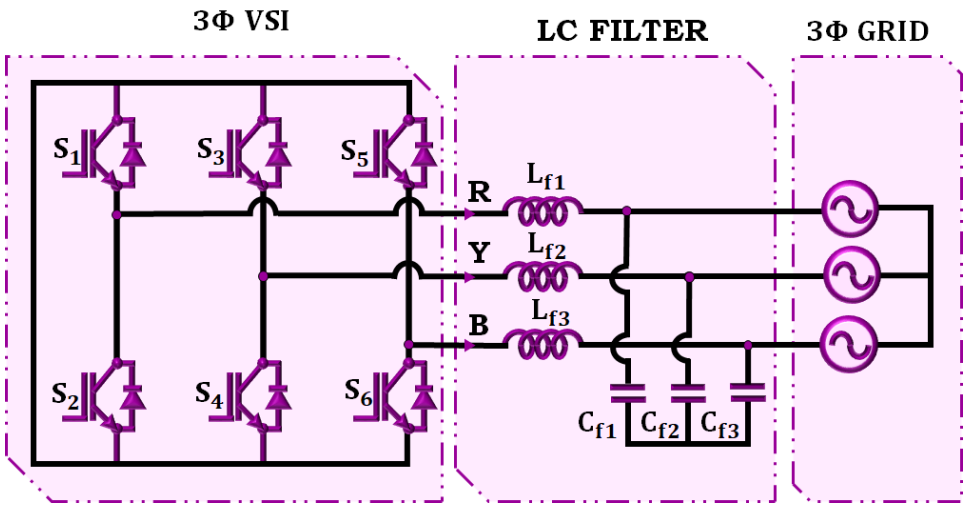

Fig.9. Three-phase VSI using dq theory-based grid synchronization.

Table 1. Parameter Specifications.

Parameter	Specifications
PV System	
No. of panels in series	14
No. of panels in parallel	7
Short circuit current	$8.95A$
Open circuit voltage	$37.25V$
Rated Power	$2.5kW$
SC-XGB	
Capacitor (C_a, C_b)	$22\mu F$
Capacitor C_0	$2200\mu F$
Inductor (L_a, L_b)	$4.7mH$
Switching Frequency	$10kHz$

low oscillations in the waveforms reflect the strength and responsiveness of the control strategy, clearly proving its efficacy in real-world applications where temperature and irradiance are never fixed.

Fig.13 visualizes the output voltage and current waveform of the northern goshawk optimized RBFNN MPPT-controlled SC-XGB converter under varying temperature and irradiance conditions. The waveforms initially exhibit fluctuations; at the same time, the SC-XGB converter readjusts its gain to achieve voltage stability on the output side. Such rapid response is also confirmed by the waveforms of both voltage and current across the converter, which indicate minimal transients followed by instant stabilization at about 600 V and 100 A, respectively. The small oscillations and quick settling time reflect the stability of the NGOA-RBFNN-MPPT controller as well as the efficiency of the converter in dealing with dynamic inputs.

Case 3: Varying temperature and Constant intensity

Fig.14 illustrates the performance of a solar PV system with condition of constant irradiance and variable temperature. PV panel's temperature rises from 28°C to 35°C at approximately 0.3s, whereas irradiance is held constant at

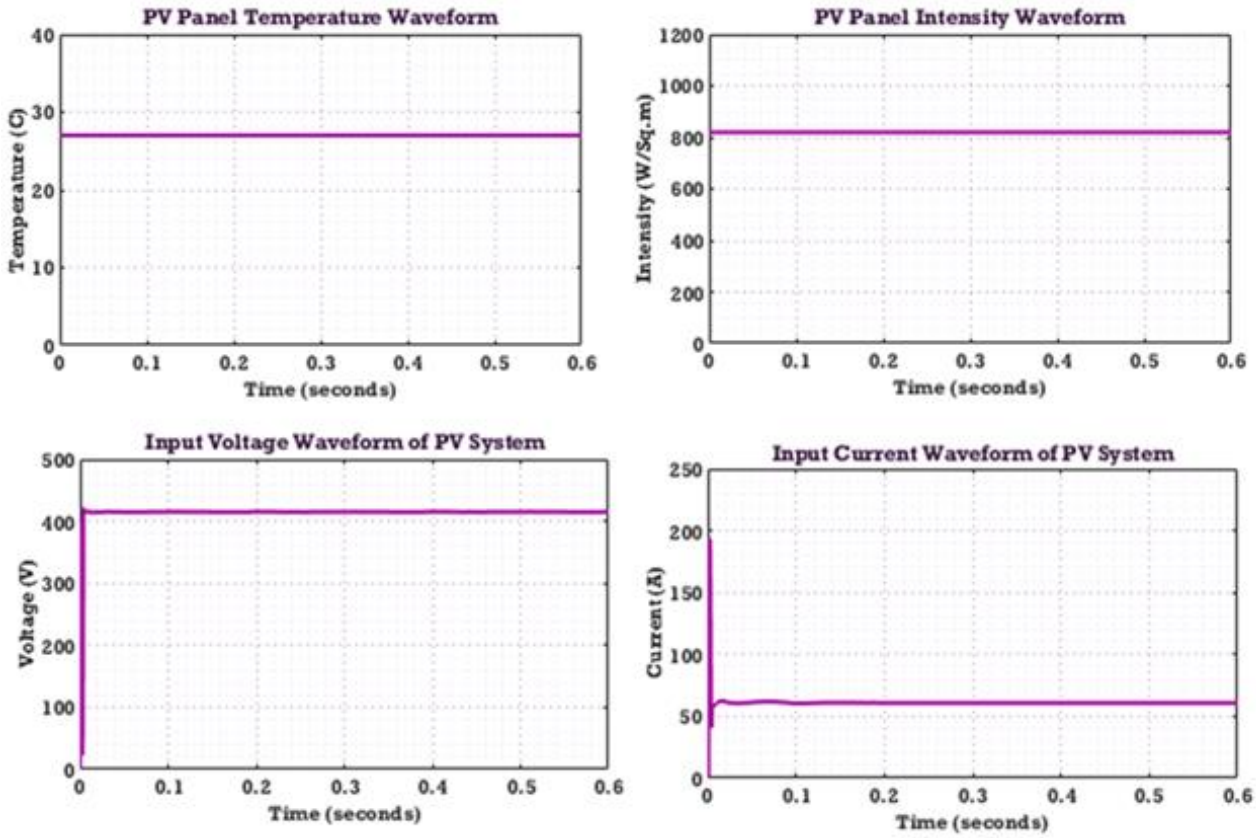

Fig. 10. PV System.

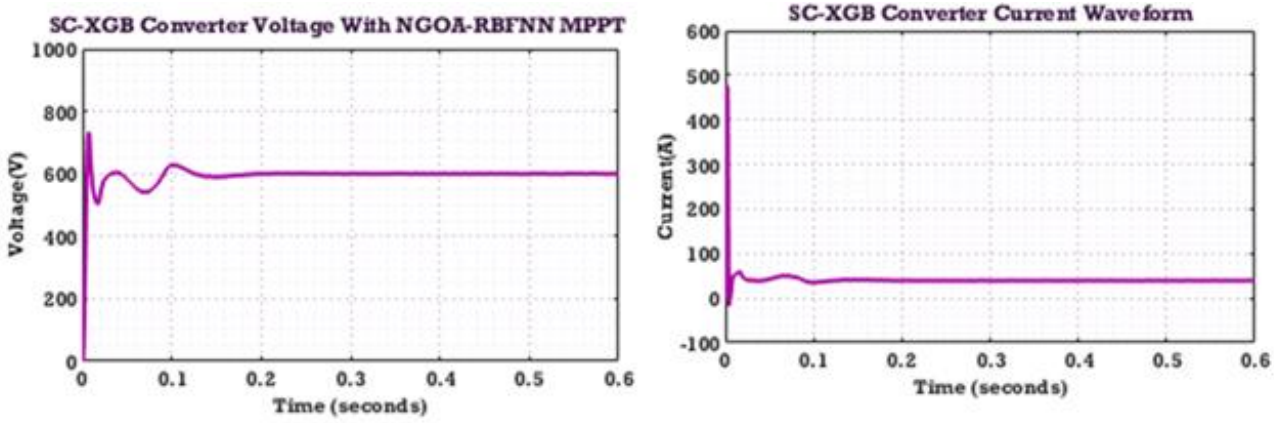

Fig. 11. Proposed converter with optimized MPPT controller.

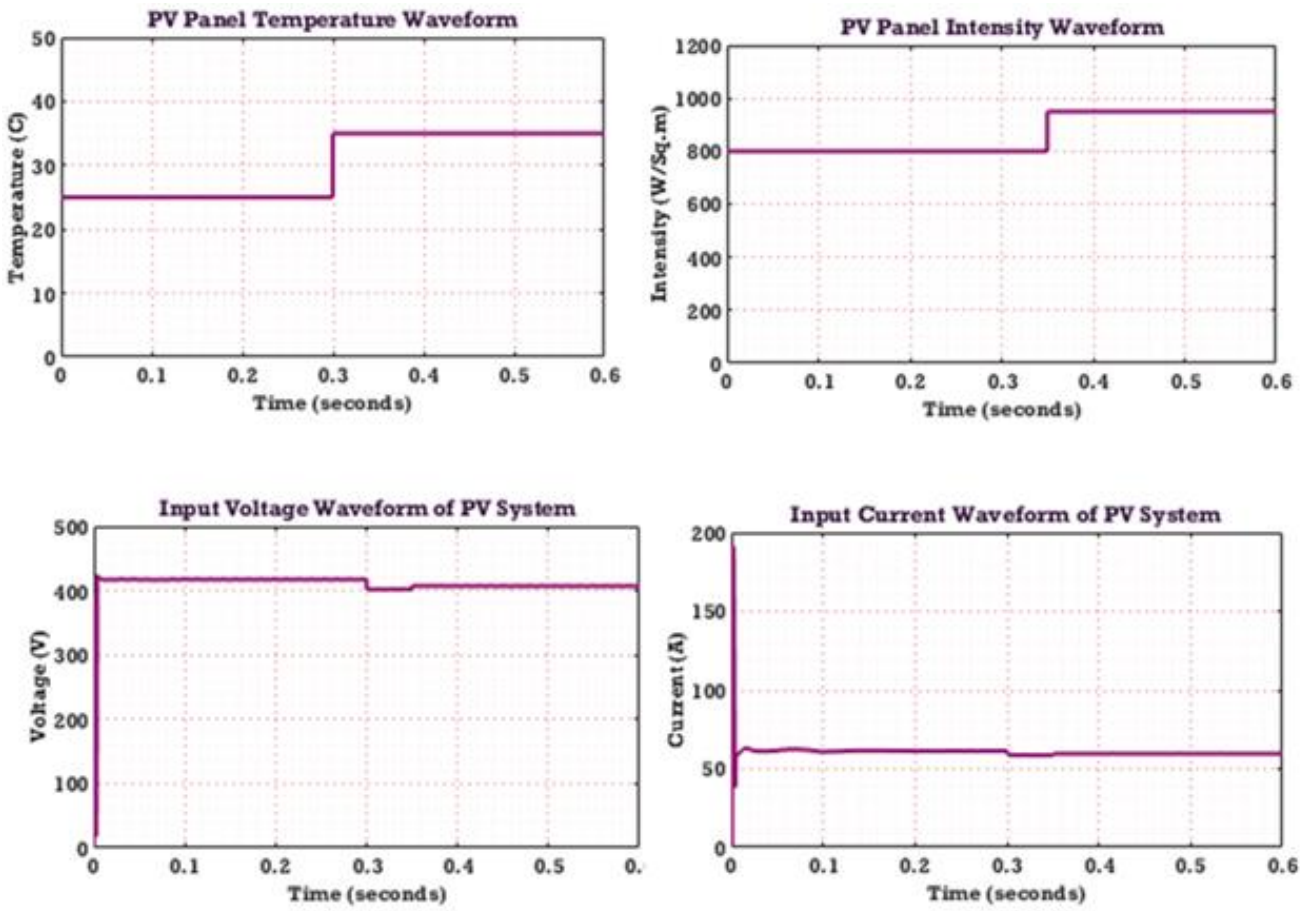

Fig. 12. PV array.

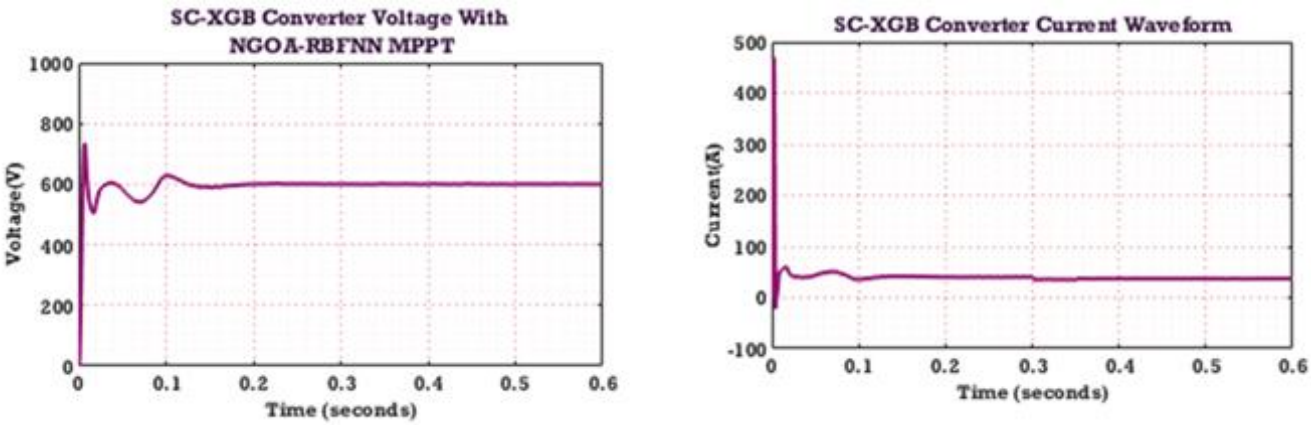

Fig. 13. Proposed SC-XGB converter with MPPT.

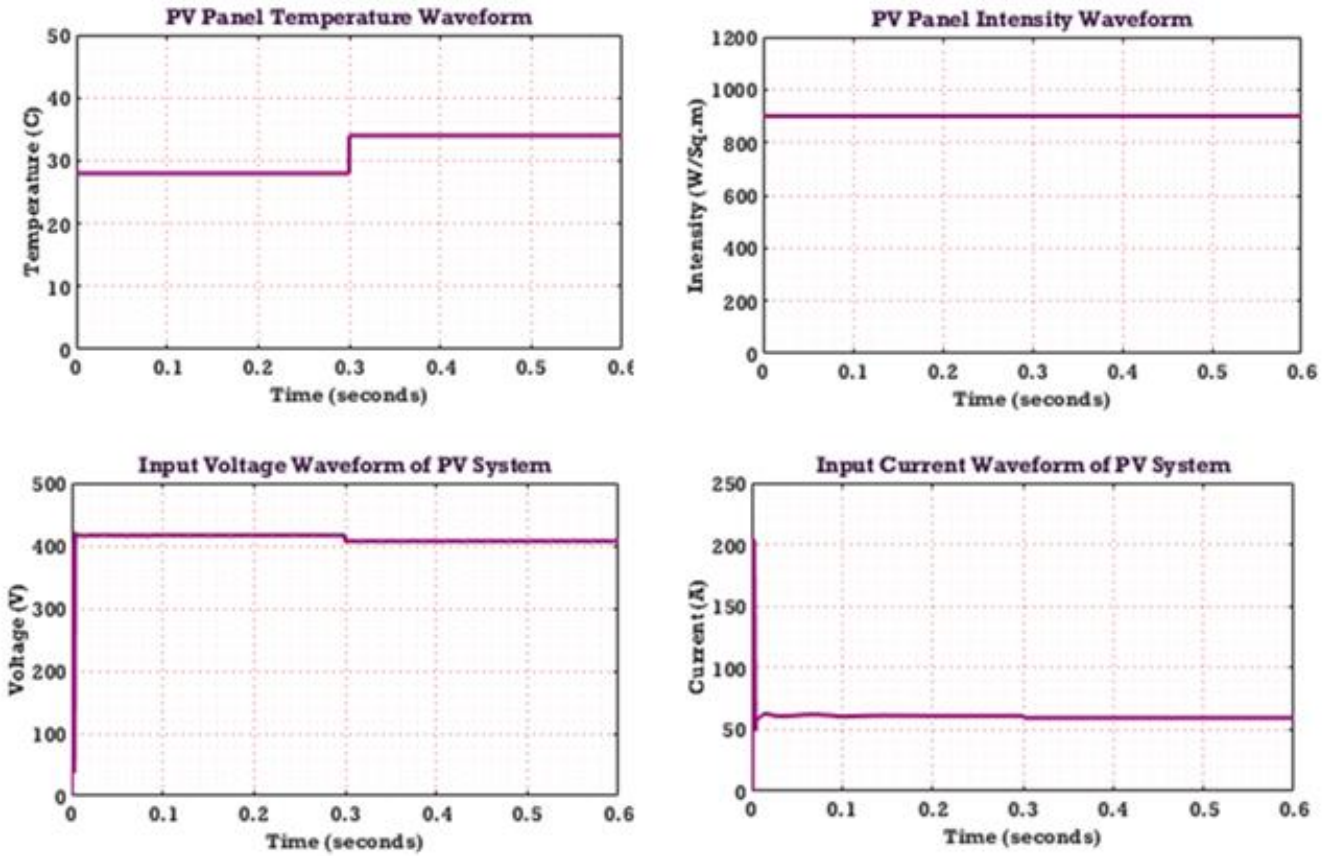

Fig. 14. PV array.

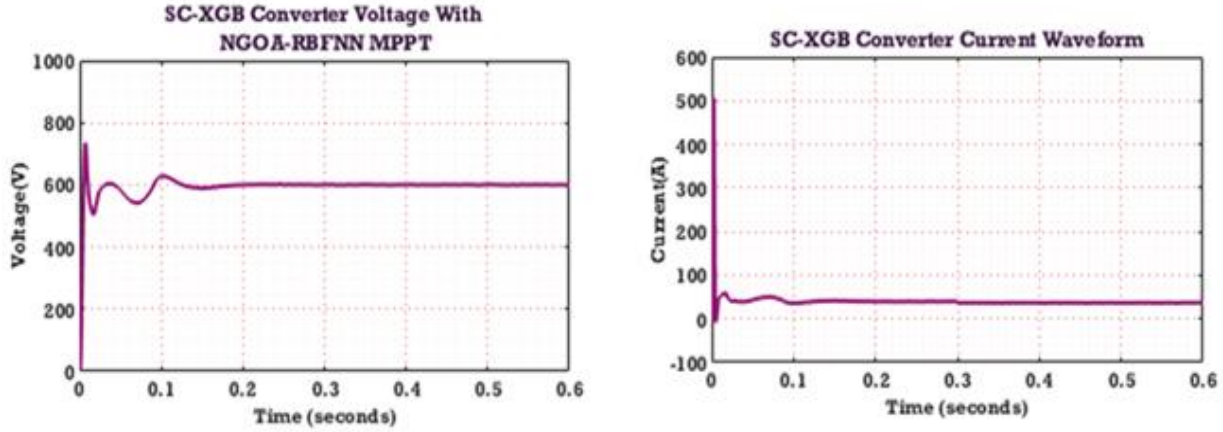

Fig. 15. SC-XGB converter with NGOA-RBFNN MPPT.

1000 W/m² during the period. Generally, a rise in temperature causes the voltage of the PV panel to decrease because of the semiconductor material's negative temperature coefficient. Then, input voltage is constant at around 35 V, and input current remains constant at about 60 A throughout the system.

Fig.15 shows the proposed SC-XGB converter with NGOA-RBFNN MPPT controlled voltage boosting responses under the condition of fluctuating temperature and fixed irradiance. The input voltage initially stabilizes at 700V before rapidly rising to a steady 600V. In parallel, the current experiences slight oscillations during startup, then settles at a constant value of 70A after approximately 0.2 seconds, despite fluctuations in PV temperature. This stable voltage and current are supplied to the converter, which, aided by

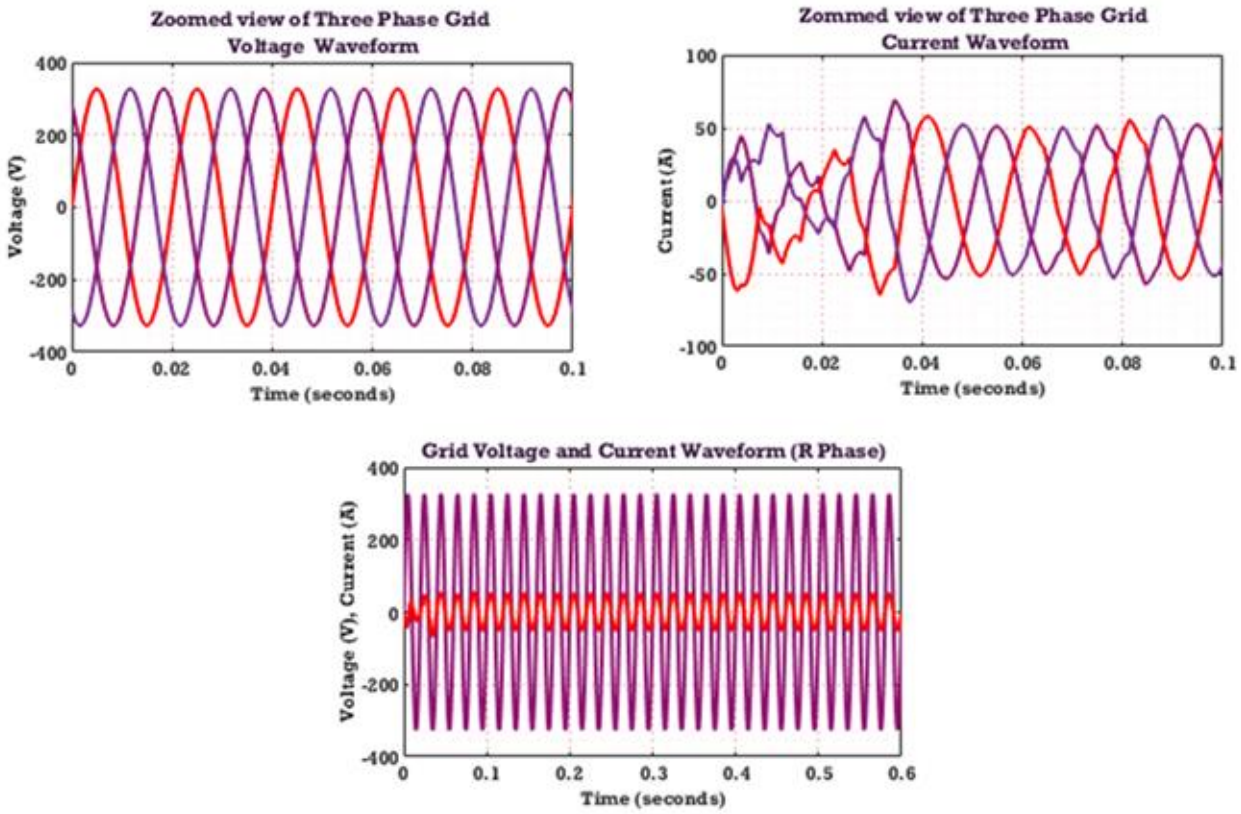

Fig. 16. Grid waveforms.

a PI controller, effectively boosts the input power. While the inherent variability of the PV system introduces minor disturbances, the converter consistently delivers an output of 600V and 70A, reaching this steady state. Such temperature stress performance reflects the combined effect of intelligent MPPT control and an improved power conversion device.

The behaviour of a three-phase grid-connected PV system with northern goshawk optimized RBFNN MPPT and SC-XGB is revealed by Fig.16. Voltage and current waveforms of the three-phase grid exhibit clean sinusoidal patterns with minimal distortion, indicating that the system is effectively synchronized with the grid. The NGOA-powered MPPT controller ensured that the PV array operated at its MPP under dynamic operations. This optimal tracking enabled the SC-XGB converter to regulate the DC output efficiently. The regulated power is then converted into AC and injected into the grid. Voltage and current waveforms of the three-phase grid show consistent amplitude and phase alignment across all three phases, confirming balanced power delivery.

Fig.17 reveals real and reactive power waveforms in a grid-connected PV system. Both waveforms start with transient oscillations when the system is trying to settle at a new operating point. These oscillations are rapidly damped, owing to the rapid convergence ability of the northern goshawk optimization algorithm incorporated in the RBFNN-MPPT controller. Once the optimal power point is reached, the system stabilizes, and both real and reactive power stabilize into constant values. The real power waveform stabilizes about a positive value, reflecting successful energy transfer from the PV system to the grid. At the same time, the waveform of the reactive power oscillates around zero after the transient state, indicating the system is running at unity power factor, a desirable state for grid-connected systems.

The Fig. 18 presents the power factor waveform, providing an insightful foretaste of the efficiency of operation in the system. The waveform first dips slightly below zero and then sharply rises above unity, typical of the transient response upon system startup or adjustment. This temporary change is a result of the inverter and control algorithms synchronizing with the grid and matching voltage and current waveforms. Nevertheless, within a fraction of a second, the power factor does stabilize exactly at 1, meaning that voltage and current are exactly in phase. This perfect PF is a direct result of intelligent coordination between the northern goshawk optimized MPPT algorithm and the SC-XGB. The MPPT ensures that the PV array is always running at its MPP, while the inverter and converter cooperate to supply clean, phase-synchronized power to the grid. Having and sustaining a power factor of 1 indicates that the system is running at maximum efficiency, reducing reactive power and losses.

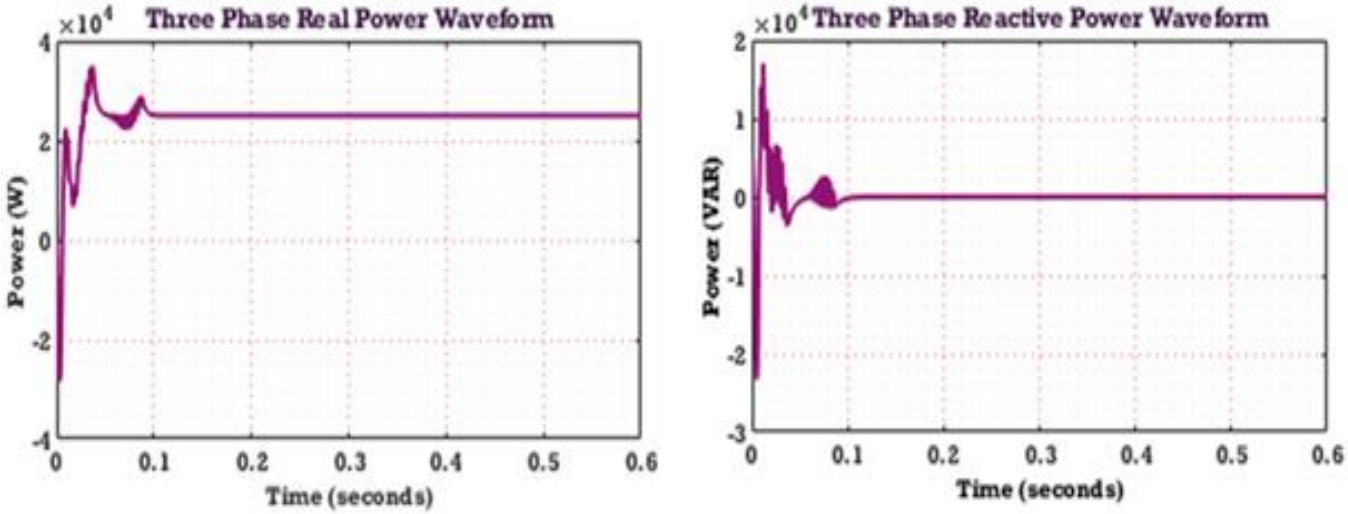

Fig. 17. Power waveforms.

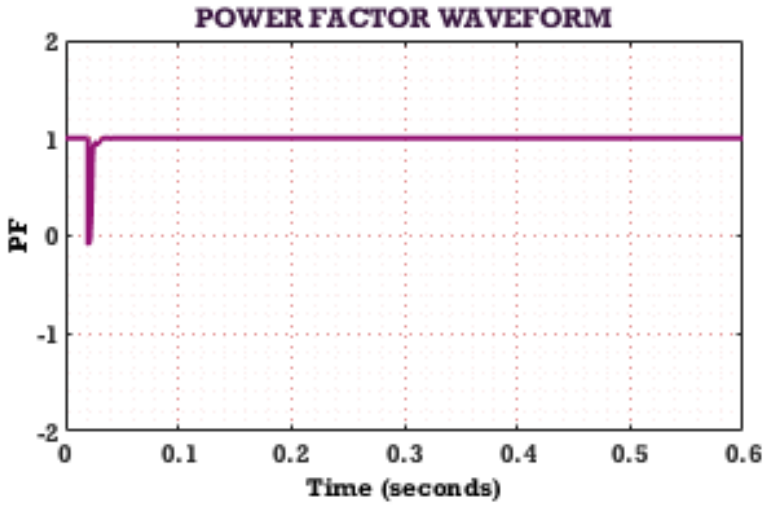

Fig. 18. PF waveform.

This performance indicates technical superiority by ensuring grid standards compliance, making system very well-suited for real-world application in smart energy grids.

Fig. 19 illustrates the THD profiles for the three-phase system. The R-phase exhibits a THD of 1.59%, while the Y-phase and B-phase register 1.62% and 1.79%, respectively. These relatively low THD levels reflect minimal harmonic interference, contributing to enhanced power quality and efficient system performance. It indicates the enhanced control provided by the northern goshawk optimization algorithm, where the MPPT controller will always be running at the maximum point of efficiency, and the SC-XGB converter and inverter cooperate to supply clean, sinusoidal output.

Fig. 20 visualizes the convergence curve comparison of optimization performances of the proposed NGOA-RBFNN MPPT, African Vulture Optimization Algorithm-Recurrent Neural Network (AVOA-RNN) [24], and RUNge kutta optimizer (RUN) [25] over 50 iterations. RUN [25] obtains the lowest fitness function at early iterations, closely followed by AVOA-RNN [24], whereas the proposed NGOA-RBFNN exhibits a relatively higher but more stable fitness function over the iterations.

Table.2 presents the comparison of tracking time for the MPPT control algorithm. The proposed approach has

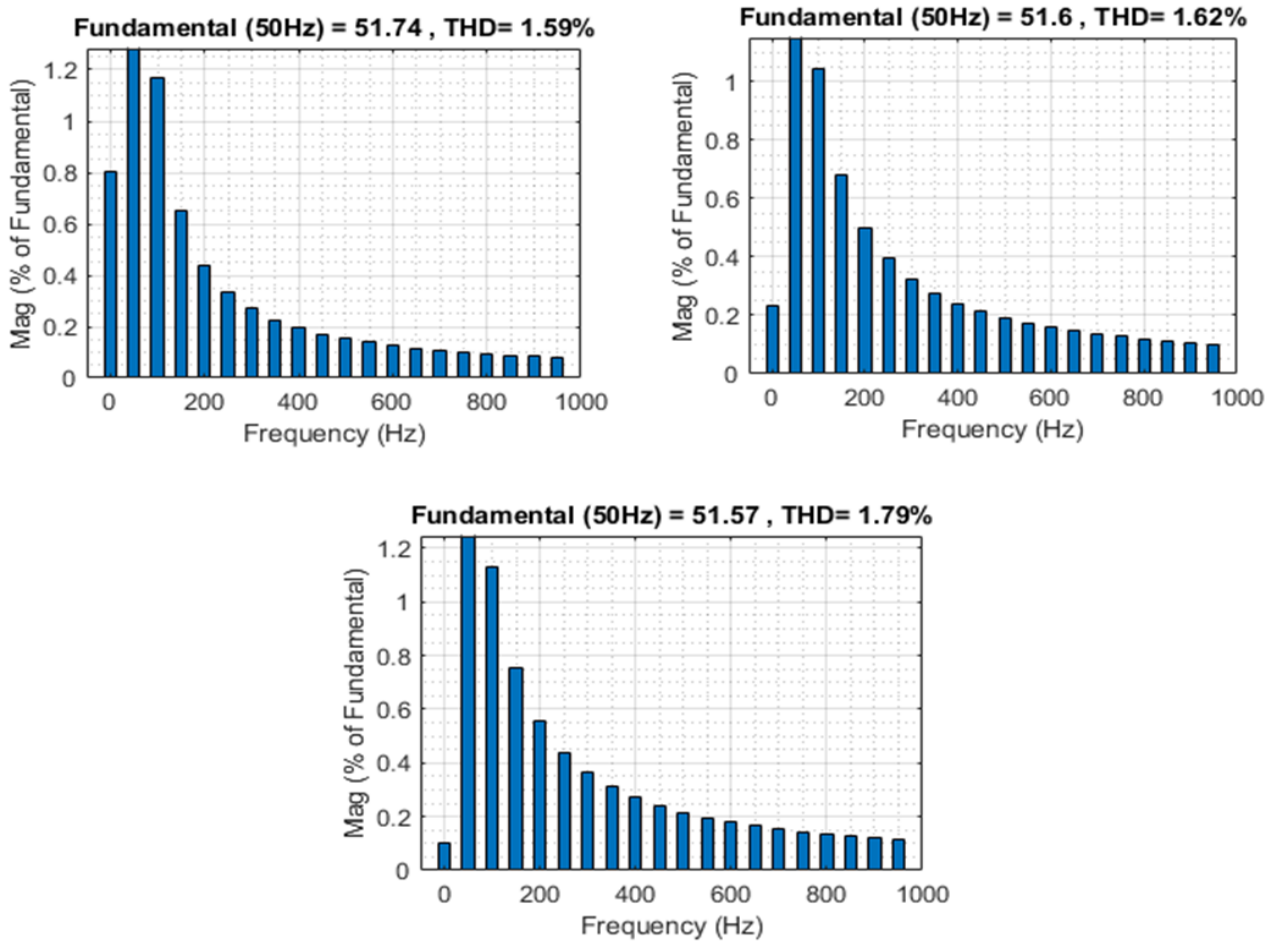

Fig. 19. THD waveforms.

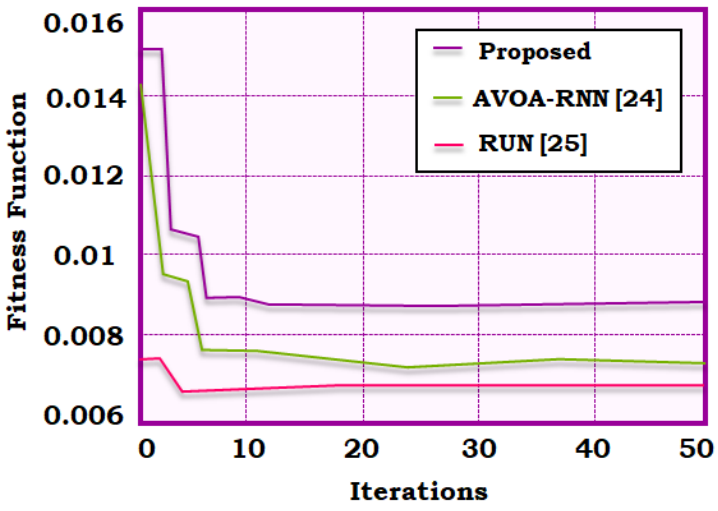

Fig. 20. Convergence curve.

Table 2. Tracking time comparison of MPPT control strategies.

MPPT Control Approaches	Tracking Time (s)
ANN-ASSPO [19]	1.52
AVOA-RNN [24]	0.6
PSO [16]	0.55
Proposed	0.10

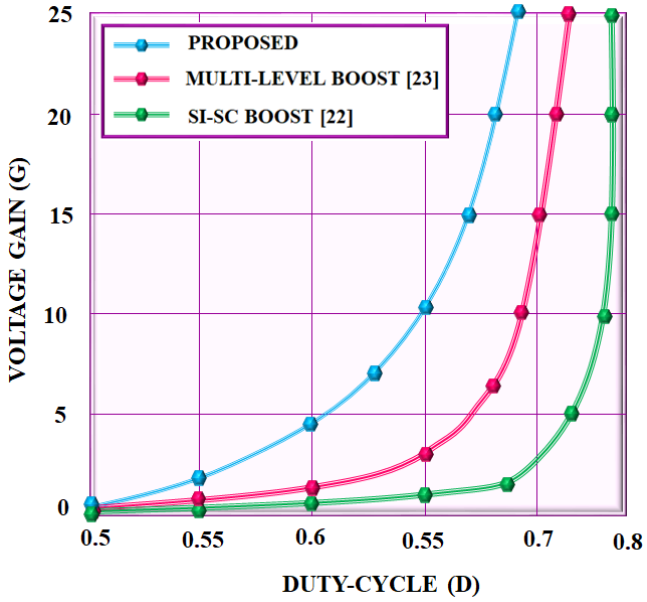

Fig. 21. Comparison of voltage gain.

the shortest settling time at merely 0.10 seconds, reflecting an extremely effective dynamic response. PSO [16] comes next with a settling time of 0.55 seconds, while AVOA-RNN [24] with 0.6s, ANN-ASSPO is at 1.52 seconds, meaning slower system stabilization. These results further support the proposed MPPT control method's efficiency from the standpoint of transient behaviour.

Fig. 21 illustrates the comparative analysis of voltage gain vs. duty cycle performance that is carried out between the proposed converter and different advanced designs, including those by Ref [22] and Ref [23]. Throughout the entire duty cycle range, the proposed converter is the top performer in terms of voltage gain. These findings reaffirm the efficacy of the proposed MPPT control method in terms of transient behaviour.

Fig. 22 presents the efficiency comparative analysis of various converter topologies; the efficiency of the proposed converter is benchmarked against existing converter topologies. Achieving a peak efficiency of 95.24%, the proposed system demonstrates superior performance. The design effectively reduces energy losses, thereby boosting overall efficiency. This underscores the capability of the proposed architecture to deliver high-performance power conversion, making it technically efficient and economically viable.

5- Conclusion

The proposed PV-grid energy management system integrates a SCXGB converter integrated with a NGOA based RBFNN MPPT controller. Together, they allow for an improved voltage gain and fast MPPT. The main innovation is in leveraging a soft-clamped high-gain converter topology and an adaptive metaheuristic-neural hybrid optimization framework, which together bring faster convergence, better tracking accuracy, and higher dynamic stability than both conventional intelligent MPPT methods and high-gain DC-

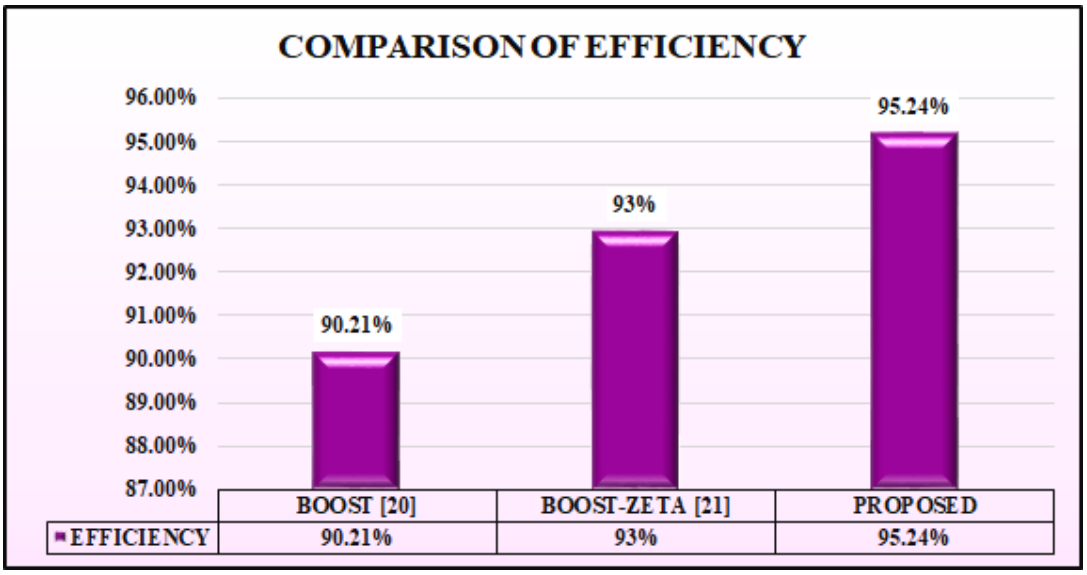

Fig. 22. Comparative analysis of efficiency.

DC converters. Simulation results in MATLAB/Simulink show that the proposed converter achieve 95.24% peak conversion efficiency, shorter transient response, and stable grid synchronization even under rapid changes in irradiance and temperature. Besides the thorough simulation studies done in the current work, experimental prototyping and Hardware-in-the-Loop (HIL) testing are being considered as future steps to prove the controller's robustness and real-time performance. In addition, a thorough investigation into the computational complexity and embedded implementation of the NGOA-RBFNN algorithm will be carried out to ensure that the solution is scalable for real grid-connected applications. Grid disturbances and parameter uncertainties, induced robustness and sensitivity analysis will be part of future work as well.

References

[1] D. P. Mishra, K. K. Rout, S. Mishra, M. Nivas, R. K. P. R. Naidu, and S. R. Salkuti, "Power quality enhancement of grid-connected PV system", International Journal of Power Electronics and Drive Systems, vol. 14, no. 1, pp. 369, 2023.

[2] K. S. Kavin, and P. Subha Karuvelam, "PV-based grid interactive PMBLDC electric vehicle with high gain interleaved DC-DC SEPIC Converter", IETE Journal of Research, vol. 69, no. 7, pp. 4791-4805, 2023.

[3] G. G. Farivar, W. Manalastas, H. D. Tafti, S. Ceballos, A. Sanchez-Ruiz, E. C. Lovell, G. Konstantinou, C. D. Townsend, M. Srinivasan, and J. Pou, "Grid-connected energy storage systems: State-of-the-art and emerging technologies", Proceedings of the IEEE, vol. 111, no. 4, pp. 397-420, 2022.

[4] S. K. Baksi, R. K. Behera, and U. R. Muduli, "Optimized 9-level switched-capacitor inverter for grid-connected photovoltaic systems", IEEE Transactions on Industry Applications, vol. 60, no. 2, pp. 3284-3296, 2023.

[5] A. Inbamani, S. U. Prabha, "Predicting the Single Diode Model Parameters using Machine Learning Model", Electric Power Components and Systems, vol. 51, no. 14, pp. 1385-1397, 2023, Taylor & Francis.

[6] B. Gunapriya, I. Abinaya, M. Karthik, and H. Vidhya, "Anti wind up PI controller with tracking for motor drive system: Modelling, simulation and implementation in lab view based FPGA", International Journal of Recent technology and Engineering, vol. 8, no. 5, 2020.

[7] K. S. Kavin, "Energy Management of AC Grid by the Solar PV System Using Landsman Converter", 2020.

[8] S. Smonia Joe Princy, C. Hentry, N. Alharbi, H. Siddiq, M. Refaei, H. Alzahrani, M. R. Bindhu, V. Sarojini, and S. Sasi Florence, "Synergistic Antimicrobial and Photocatalytic Properties of PVP-Ag-PEG Nanocomposites for Sustainable Leachate Treatment", Journal of Inorganic and Organometallic Polymers and Materials, pp. 1-19, 2024.

[9] S. V. K. Naresh, S. Peddapati, and M. L. Alghaythi, "A novel high quadratic gain boost converter for fuel cell electric vehicle applications", IEEE Journal of Emerging and Selected Topics in Industrial Electronics, vol. 4, no. 2, pp. 637-647, 2023.

[10] S. Pirpoor, S. Rahimpour, M. Andi, N. Kanagaraj, S. Pirouzi, and A. H. Mohammed, "A novel and high-gain switched-capacitor and switched-inductor-based DC/DC boost converter with low input current ripple and mitigated voltage stresses", IEEE Access, vol. 10, pp.

32782-32802, 2022.

[11] P. L. Rose, V. Sarojini, and G. D. Biji, "Antibacterial and anticancer activity of green synthesised silver nanoparticles using polysaccharides extracted from the marine alga Portieria hornemannii", Journal of Applied & Natural Science, vol. 16, no. 1, 2024.

[12] K. S. Kavin, P. S. Karuvelam, N. Kumar, S. Kar, R. A. Rahiman, and S. Patwa, "Coupled inductor interleaved boost converter with ANN and RNN based MPPT algorithm for PV system", International Journal of Applied Power Engineering (IJAPE), vol. 13, no. 3, pp. 616-627, 2024.

[13] A. K. Priya, and A. Yazhini. "Integrating Whale Optimization Algorithm and Machine Learning for Efficient Traffic Management",

[14] A. I. M. Ali, H. H. Mousa, H. R. A. Mohamed, S. Kamel, A. S. Hassan, Z. M. Alaas, E. E. Mohamed, and A. R. Y. Abdallah, "An enhanced P&O MPPT algorithm with concise search area for grid-tied PV systems", IEEE Access, vol. 11, pp. 79408-79421, 2023.

[15] A. Hilali, Y. Mardoude, A. Essahlaoui, A. Rahali, and N. El Ouanjli, "Migration to solar water pump system: Environmental and economic benefits and their optimization using genetic algorithm Based MPPT", Energy Reports, vol. 8, pp. 10144-10153, 2022.

[16] A. O. Baatiah, A. M. Eltamaly, and M. A. Alotaibi, "Improving photovoltaic MPPT performance through PSO dynamic swarm size reduction", Energies, vol. 16, no. 18, pp. 6433, 2023.

[17] O. M. H. Anssari, M. Badamchizadeh, and S. Ghaemi, "Designing of a PSO-based adaptive SMC with a multilevel inverter for MPPT of PV systems under rapidly changing weather conditions", IEEE Access, vol. 12, pp. 41421-41435, 2024.

[18] M. A. Kamarposhti, H. Shokouhandeh, and I. Colak, "Optimization of Adaptive Fuzzy Controller for Maximum Power Point Tracking Using Whale Algorithm", Computers, Materials & Continua, vol. 73, no. 3, 2022.

[19] K. Krishnaram, T. S. Padmanabhan, F. Alsaif, and S. Senthilkumar, "Performance optimization of interleaved boost converter with ANN supported adaptable stepped-scaled P&O based MPPT for solar powered applications", Scientific Reports, vol. 14, no. 1, pp. 8115, 2024.

[20] G. G. Ramanathan, and N. Urasaki, "Non-isolated interleaved hybrid boost converter for renewable energy applications", Energies, vol. 15, no. 2, pp. 610, 2022.

[21] X. Fang, X. Lai, X. Wang, and H. Zhao, "The High Voltage Gain Coupled Inductor Boost-Zeta DC/DC Converter", CPSS Transactions on Power Electronics and Applications, vol. 9, no. 2, pp. 127-140, 2024.

[22] S. Pirpoor, S. Rahimpour, M. Andi, N. Kanagaraj, S. Pirouzi, and A. H. Mohammed, "A novel and high-gain switched-capacitor and switched-inductor-based DC/DC boost converter with low input current ripple and mitigated voltage stresses", IEEE Access, vol. 10, pp. 32782-32802, 2022.

[23] J. C. Rosas-Caro, J. E. Valdez-Resendiz, G. Escobar, and F. Beltran-Carbajal, "A multilevel boost converter with reduced inductor current", Electronics, vol. 12, no. 22, pp. 4585, 2023.

[24] C. Jiang, "African vulture optimized RNN algorithm maximum power point tracking (MPPT) controller for photovoltaic (PV) system", Measurement: Sensors, vol. 36, pp. 101392, 2024.

[25] K. M. AboRas, A. H. Alhazmi, and A. I. Megahed, "Optimal Incremental Conductance-Based MPPT Control Methodology for a 100 KW Grid-Connected PV System Employing the RUNge Kutta Optimizer", Sustainability, vol. 17, no. 13, pp. 5841, 2025.

HOW TO CITE THIS ARTICLE

V. Babu, T. Sridevi, M. J. Murali, J. Gnanavel, D. Dinesh, M. Balasubramanian, NGOA Assisted Neural Network MPPT for Grid-Connected PV System with Soft-Clamp X-Gain Boost Converter, AUT J. Elec. Eng., 58(3) (2026) 489-508.

DOI: 10.22060/eej.2026.25230.5872